Int. J. Heat Mass Transfer. Vol. 21, pp. 371–384. Pergamon Press 1978. Printed in Great Britain

MASS, MOMENTUM, AND ENERGY TRANSPORT IN TURBULENT FREE JETS

PASQUALE M. SFORZA* and ROBERT F. MONS†
Polytechnic Institute of New York, Aerodynamics Laboratories Farmingdale, NY 11735, U.S.A.

(*Received* 8 *March* 1976 *and in revised form* 18 *December* 1977)

Abstract—An experimental and analytic investigation of mass, momentum, and heat transfer in a free turbulent flow field is presented. In particular, the case of a jet issuing from a circular orifice into the free ambient atmosphere of a laboratory room is studied. Three basic flow conditions are considered: (1) isothermal mixing of an air jet with the surroundings, (2) isothermal mixing of a binary mixture (air/CO_2) jet with the surroundings, (3) nonisothermal mixing of a heated air jet with the surroundings. Specially designed aspirating probes are used to measure the mean fluxes of mass, momentum and total enthalpy. These properties are considered to be the dependent variables defining the flow field. Accurate measurements of the more usual variables, such as mean species mole fraction, mass-averaged mean velocity and mean temperature are a by-product of the raw data from the aspirated probes.

The normalized results indicate that, for identical initial conditions the flux of mass and the flux of total enthalpy behave identically and that both of these variables decay faster and have larger halfwidths than does the momentum flux. However, the radial coordinate at which the value of the flux variable is sensibly equal to zero, that is, the mean "edge" of the jet, is found to be the same for all flux variables.

An extended version of the Reichardt inductive theory of free turbulence is found to adequately predict the entire flowfield for all of the conserved flux variables.

NOMENCLATURE

C, $2\pi\int_0^\infty \overline{\rho_C u}\, r\, dr$, integral of CO_2 mass flux;
d, diameter of jet orifice;
h, enthalpy;
h_T, total enthalpy;
Δh_T, $h_T - h_\infty$;
H, $2\pi\int_0^\infty \overline{\rho u \Delta h_T}\, r\, dr$, integral of enthalpy flux;
m, $2\pi\int_0^\infty \overline{\rho_A u}\, r\, dr$, integral of air mass flux;
m_i, mass flow of mixture through orifice;
M, $2\pi\int_0^\infty \overline{\rho u^2}\, r\, dr$, integral of momentum flux;
P, pressure;
Q, source quantity defined in Table 1;
Q_e, generalized energy source function;
r, radial coordinate;
$r_{1/2}$, halfwidth;
T, temperature;
T_T, total temperature;
ΔT_T, $T_T - T_\infty$;
u, axial velocity component;
v, radial velocity component;
$\dot{w}_i$, mass rate of production of species i;
x, axial coordinate;
$\bar{x}$, x/d;
x_0, virtual origin;
X_i, mole fraction of species i;
Y_i, mass fraction of species i;
Y_f, mass fraction of species other than ambient species.

Greek symbols

$\Lambda(x)$, generalized transfer coefficent, equation (3);
φ, quantity defined in Table 1;
ρ, density;
χ, transformed axial coordinate, equation (8);
$\bar{\chi}$, χ/d;
θ, $d(\rho_\infty/\rho_e)^{-1/2}$.

Subscripts

A, denotes air;
C, denotes carbon dioxide;
$\mathcal{L}$, denotes centerline;
e, denotes ceterline conditions at exit;
i, denotes jet exit conditions;
∞, denotes ambient conditions.

Superscripts

$\bar{}$, denotes time-averaged quantity;
$'$, denotes fluctuation quantity.

*Professor.

†Research Associate, presently at Westinghouse Ocean Engineering Research Center.

1. INTRODUCTION

A RECENT workshop on nonhomogeneous turbulent mixing [1], provides an excellent review of the leading edge of research on such flows; other conference proceedings also yield a good overview [2, 3]. Particularly impressive is the sophistication of the experimental techniques required to probe the detailed structural aspects of these flows as well as the enormous difficulties faced by analytical modelers [4–8]. The objective of this investigation is to approach the problem of mass, momentum, and heat transfer in a turbulent jet from a very simplified point of view.

It is becoming increasingly clear that there is developing a divergence between analysis and experiment, if only because these groups are focusing upon two different sets of dependent variables. In this spirit, we wish to set down some of our experiences with one of the first approaches to the problem of free turbulence that departed from the accepted norm: the inductive theory of free turbulence due to Reichardt [9].

It is our intent to show the outcome of this basic concept, extended by Baron and Alexander [10], of treating the mean fluxes of mass, momentum, and energy as the dependent variables in free mixing problems. This effort was prompted by a desire to exploit the simplicity of the analytic aspects of the theory, to provide a reasonably unified attempt at assessing the value of the theory for academic completeness, to capitalize on the possibility of developing simplified diagnostic equipment for such complex flow problems, and of course by a curiosity as to the extent to which the theory could continue to yield the accuracy that we (and others) had found in years of familiarity with it.

The flow field to be considered in this work is the turbulent, incompressible, axisymmetric free jet. Three basic cases are treated: (a) an isothermal homogeneous jet (the "cold" jet); (b) an isothermal nonhomogeneous jet (the "binary" jet); (c) a nonisothermal homogeneous jet (the "hot" jet). The variable density cases studied included situations with reasonably large initial density differences (greater than 25%) so that the density effects considered are not entirely passive. A new type of isokinetic sampling probe was developed which allowed all the pertinent flux variables to be deduced with that instrument alone so that sequential measurements at a given location could be performed. Furthermore, the conventional kind of dependent variables such as velocity, temperature, and concentration could also be deduced from the raw data with what appears to be reasonable accuracy.

First the basic concept of the inductive theory in an extended form is discussed and the solutions pertinent to the present cases are derived. Then the special flux sampling probe developed for this investigation is described and evaluated. Next, the three fundamental cases mentioned above are treated in detail and the experimental results are compared with the theory. Following this the special combined result of the study, such as mass entrainment, and the results for the conventional flow variables are discussed.

2. DISCUSSION OF THE EXTENDED REICHARDT ANALYSIS

For the condition of steady two-dimensional or axisymmetric flow, the conservation equations can be expressed, with the use of the global continuity equation and after the usual time-averaging, in the general form listed below:

$$\frac{\partial}{\partial x}\overline{(\rho u\varphi)} + \frac{1}{r^j}\frac{\partial}{\partial r}\left[r^j\overline{(\rho u\varphi)}\right] = \bar{Q}, \tag{1}$$

where $j = 0$ for two-dimensional flow and $j = 1$ for axisymmetric flow. Table 1 lists the variables which may be represented by φ and Q where molecular transport and body forces are neglected.

Table 1

Quantity	φ	Q
Species mass	Y_i	$\dot{w}_i$
Momentum	u, v	$-\frac{\partial P}{\partial x}, -\frac{\partial P}{\partial r}$
Energy	$h_t - h_s$	Q_e

Note that the system of equation (1) will be devoid of the usual correlations of turbulent flow if the quantities within the parentheses are treated as a single variable.

When equation (1) is integrated over all space, we obtain

$$\frac{\partial}{\partial x}\int\int_0^\infty \overline{(\rho u\varphi)}\,\mathrm{d}A = \int\int_0^\infty \bar{Q}\,\mathrm{d}A. \tag{2}$$

Hence, in the absence of generation terms such as pressure gradients, chemical reactions, heat addition, etc., equation (2) states that the total flux of each quantity originates entirely at the initial station and is invariant.

The crux of the present analysis lies in the suggestion made by Reichardt [9] and generalized by Baron and Alexander [10] that

$$\overline{\rho v\varphi} = -\Lambda(x)\frac{\partial\overline{(\rho u\varphi)}}{\partial r}. \tag{3}$$

Thus the system described by equation (1) becomes

$$\frac{\partial}{\partial x}\overline{(\rho u\varphi)} - \frac{\Lambda(x)}{r^j}\frac{\partial}{\partial r}\left[r^j\frac{\partial}{\partial r}\overline{(\rho u\varphi)}\right] = \bar{Q}. \tag{4}$$

This equation is analogous to the equation for heat conduction where diffusivity is a function of time and heat is generated within the system. If Q is linear in the dependent variable, then the equation is linear and may be treated by many well known analytical techniques with the specification of the proper boundary and initial conditions. Rather arbitrary conditions may be specified at the initial station; this permits analysis of many geometrical configurations and the attendant initial distributions of $\rho u\varphi$.

Solutions of the system of equation (4) is straightforward so that only a brief outline of the procedure is necessary here. We seek solutions for the case of no generation terms when these equations take the form

$$\frac{\partial}{\partial x}(\overline{\rho u\varphi}) = \frac{\Lambda(x)}{r}\frac{\partial}{\partial r}\left[r\frac{\partial}{\partial r}(\overline{\rho u\varphi})\right] \tag{5}$$

where $\varphi = u, h_t - h_\infty$ or Y_f, and with initial conditions

$$\text{at} \quad x = 0: \quad \overline{\rho u\varphi} = \begin{cases} f_\varphi(r') & \text{for } r' < \dfrac{d}{2} \\ 0 & \text{for } r' \geqslant \dfrac{d}{2} \end{cases} \tag{6}$$

and boundary condition

$$\overline{\rho u\varphi} \to 0 \quad \text{as } r \to \infty. \tag{7}$$

Here, d is the diameter of the orifice.

The parameter $\Lambda(x)$ is unknown and must be obtained by comparison between theory and experiment. We extend the Reichardt approach still further by introducing the transformation

$$\chi = \int_0^x \Lambda(x')\,dx' \tag{8}$$

or

$$d\chi = \Lambda(x)\,dx,$$

Under the transformation (8), equation (5) becomes

$$\frac{\partial(\overline{\rho u\varphi})}{\partial\chi} = \frac{1}{r}\frac{\partial}{\partial r}\left[r\frac{\partial}{\partial r}(\overline{\rho u\varphi})\right]. \tag{9}$$

The solution of (9) for arbitrary initial conditions is

$$\overline{\rho u\varphi} = \frac{1}{2\chi}\exp-\left\{\frac{r^2}{4\chi}\right\}\int_0^{d/2}\exp-\left\{\frac{r'^2}{4\chi}\right\} \times I_0\left(\frac{rr'}{2\chi}\right)f_\varphi(r')r'\,dr' \tag{10}$$

where $I_0(rr'/2\chi)$ is a modified Bessel function of order zero. The specific solution for each case indicated above is obtained by specification of each initial condition $f_\varphi(r')$ and specification of the form of the transformation (8).

Note that $\Lambda(x)$ may be a different function for each of the dependent variables represented by φ. Such would be the case if there is a different rate of mixing, as the term is usually applied, for each of the dependent variables. Upon application of the transformation represented by equation (8), however, a single form for the governing equations is obtained. Thus, in the transformed system of coordinates, the only difference in the solution for each of the dependent variables is the result of different initial conditions, and for identical initial conditions, the solutions for each of the variables are identical. In the inductive theory, difference in the rates of mixing are manifested only in the form of the transformation between $\bar{x}$ and $\bar{\chi}$.

The property of the inductive theory discussed above can be used to establish the extent to which preferential mixing exists for the flux variables. Comparing the transformation between $\bar{x}$ and $\bar{\chi}$ is especially useful because of the ability of the inductive theory to account for variation in centerline decay and halfwidth growth that is a result of differences in initial conditions. Thus, in this work, a difference in the rate of turbulent mixing will be defined as a difference in the transformation between $\bar{x}$ and $\bar{\chi}$, and a quantity A will be said to mix faster than a quantity B if for a given value of $\bar{x}$ the corresponding value of $\bar{\chi}$ for quantity A is greater than the corresponding value of $\bar{\chi}$ for quantity B.

3. DEVELOPMENT OF EXPERIMENTAL TECHNIQUES TO MEASURE FLUX VARIABLES

(A) *The basic mass flux probe*

The concept underlying the mass flux probe was the capture of a mean streamtube with the same diameter as the inside diameter of the probe; in the ideal case the static pressure at the probe entrance should equal the free stream static pressure. By locating static pressure taps near the inlet of the probe it would be possible to determine when the above condition is satisfied. Once the condition of isokinetic sampling is achieved a flow meter could be used to quantitatively fix the mass flow passing through the probe; since the area of the inside of the probe is known, the local mass flux $\overline{\rho u}$ may be determined.

Of course, the geometry of the inlet, among other things, can seriously affect the actual pressure measured at the probe entrance. In addition, the construction of a small (1.6 mm OD) probe, necessary for good resolution, dictates a simple inlet design to avoid impossible manufacturing situations. To evaluate different inlet geometries a larger (6.4 mm OD) probe was constructed incorporating removable inlets and placed in the test section of a low turbulence wind tunnel. A venturi upstream of the vacuum pump was used as a flow meter and the inlet static pressure was continually monitored along with the test section static pressure by means of an inclined manometer. These evaluations were performed over a range of velocity of approximately 3–22 m/s, and in all cases a good correlation between the inlet pressure and the mass flux for the isokinetic sampling condition was noted.

Five different inlet geometries were investigated; the design which was finally chosen is shown in Fig. 1. The pressure taps were located immediately behind the end of the inlet radius; this gave a reading slightly below free stream static pressure at the isokinetic sampling condition. To achieve the desired pressure reading it was only necessary to patiently enlarge the inside diameter of the inlet with a tapered reamer to a very slight extent.

If no sample is withdrawn the probe becomes an impact tube and the pressure measured at the inlet taps is effectively the mean total pressure of the flow. Thus it is seen that the probe sensitivity is proportional to the square of the velocity of the flow. The accuracy of the probe depends upon the accuracy of the pressure readings and the flow meter and can be about 1%. Sensitivity to yaw was also investigated and the probe

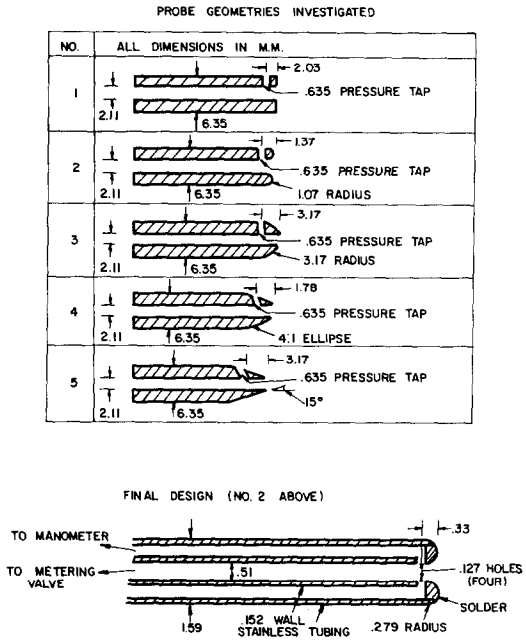

FIG. 1. Mass flux probe inlet geometries tested and details of final design.

used was fairly insensitive up to angles of about 20°, i.e. about the same sensitivity to yaw as an impact tube.

The miniature probe derived from the larger scale experiments described above has an inside cross-sectional area of 1.96×10^{-3} cm^2. The range of velocities to be measured in the jet flows was from essentially zero up to about 66 m/s. Thus it was necessary to build a system to regulate and measure a very small mass flow. In addition the flow meter had to measure the flow for various gas mixtures and for various flow temperature. Several different techniques were considered for the quantitative measurement of the mass flow; because of the intent to study non-homogeneous, nonisothermal flows, a calibrated needle valve was finally chosen as the flow meter, primarily for its versatility. The actual valve used was a Nupro very fine needle valve with a micrometer handle. The bore was enlarged and a new needle fabricated to achieve the desired flow rates. The micrometer handle allowed readings to three significant figures.

Calibration was performed by evacuating a chamber of known volume and then filling the chamber through the valve at a constant setting to a pressure of about 250 mm Hg; measuring the time necessary to fill the chamber allows computation of the mass flow. For consistency, the valve was calibrated while connected to the probe. Due to minute machining flaws a considerable number of data points were necessary for good calibration. The reader is advised that there is considerable difficulty in such a calibration and an alternate flow meter would be desirable.

With no internal flow the mass flux probe becomes an impact tube. The mean total pressure thus measured can, with the knowledge of the mean static pressure, yield a reasonable inference as to the mean square velocity $\overline{u^2}$. The mass flux probe itself measures $\overline{\rho u}$, or $\bar{u}$ in a constant density flow. Thus it is possible to deduce a reasonable estimate of the turbulence intensity in a constant density flow with this mean measurement device from the relation

$$\overline{u'^2} = \overline{u^2} - \bar{u}^2$$

provided that the measurements can be performed with sufficient accuracy. Note that this equation involves the differences of squares and errors will be greatly amplified. If reasonable results are obtained for the intensity, it appears safe to conclude that the mass flux probe is an accurate device for measurements in turbulent shear flows.

Using the method described above, profiles of intensity, nondimensionalized with respect to the centerline velocity, are shown for the isothermal homogeneous jet described in Section 4, as a function of r/x for various x/d locations in Fig. 2, and are compared to the hot-wire results of Wygnanski and Fiedler [11]. While there is noticeable scatter in a given profile, the overall results are considered quite good. This technique will be pursued in future studies and these simple results are presented here only for

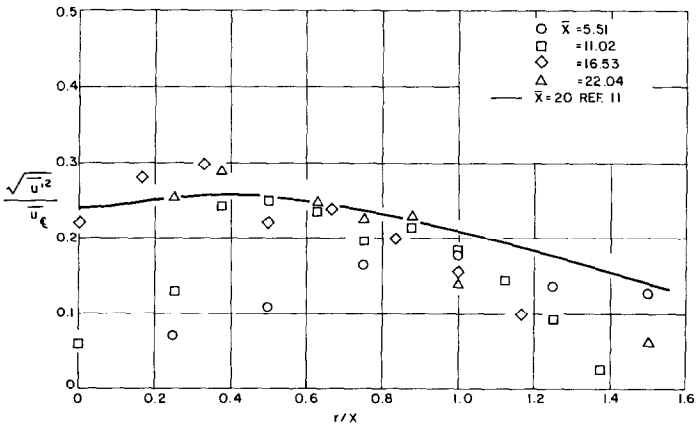

FIG. 2. Intensity of axial velocity fluctuations deduced from mass flux probe measurements. Curves shown for comparison are indicative of hot wire measurements reported in [11].

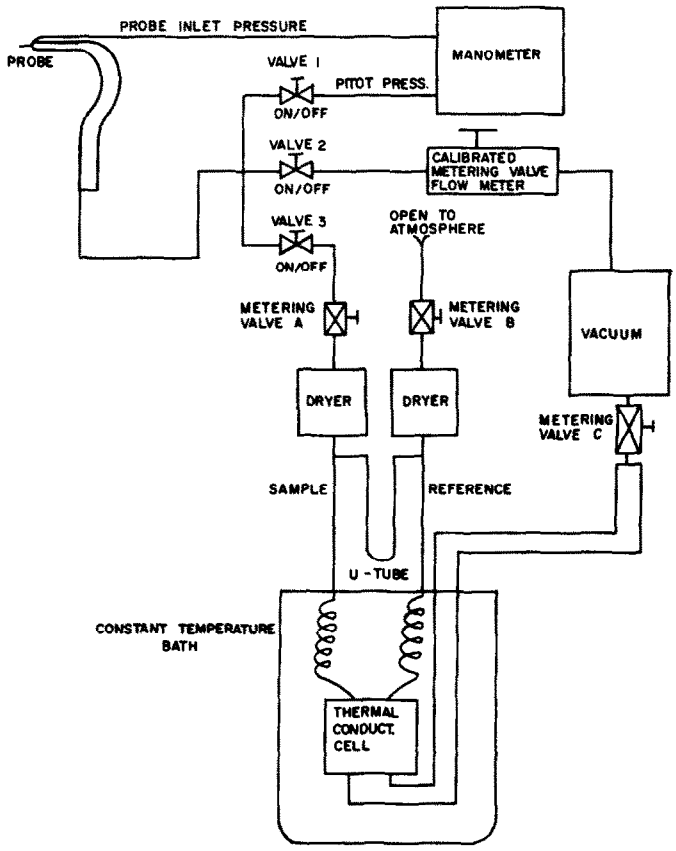

FIG. 3. Schematic diagram of gas sampling and analysis system.

purposes of illustrating the practicality of the mass flux probe.

(B) *The system for species mass flux measurements*

The gas analyzer constructed for the present work is a dynamic system employing a termistor element thermal conductivity cell manufactured by the Carle Instrument Corporation. The distinguishing feature of this system is that the mass flux probe metering system is incorporated so that the total mass flux of the flow is analyzed without changing the sampling rate at the probe itself. A schematic diagram of the gas analyzer is shown in Fig. 3. The gas analyzer indicates the mole fraction of the contaminent species (carbon dioxide in the present quasi-binary mixture); this provides the correction factor for the total mass flux measurement recorded previously and the mass fraction of the species in question. The product of the mass fraction of a given species and the total mean mass flux gives a reasonably accurate measure of the relevant species mass flux, when the sample is well mixed. Thus all quantities of interest here, for the case of an isothermal flow of a binary gas mixture, namely the momentum flux, ρu^2, the mass flux of carbon dioxide, $\rho_C u$, and the mass flux of air, $\overline{\rho_A u}$, may be inferred from measurements made with one probe, essentially simultaneously.

(C) *The system for enthalpy flux measurements*

A calorimetric probe employs a coolant and a simple energy conservation principle to measure the energy content of a flow. A modified version of a commercial calorimetric probe manufactured by the Greyrad Corp. was originally considered for the enthalpy flux measurements in this investigation. The Greyrad probe was designed for high heat flux applications such as plasma diagnostics; as a consequence several problems arose during the course of calibration that precluded the use of this probe for the present low heat flux cases.

A new calorimetric probe which directly incorporated the previously described mass flux probe was designed and constructed. This probe was made by machining a spiral channel into the outside wall of a copper tube and then shrink fitting this tube into a stainless steel tube. The new design insulated the coolant inlet as much as possible and the internal thermocouples were made to be adjustable within the probe; both these improvements were made to try to improve the performance based upon the experience with the Greyrad probe. In addition the new probe had the special mass flux measuring inlet as an integral part.

Even after all the care in design and manufacture it was found that the enthalpy flux calibrations made with this new probe in the potential core region of a heated jet were disappointing. It was determined that most of the heat was being conducted away by the probe body rather than being transferred to the coolant. This was the basic problem with the calorimetric types of probe. To eliminate this conductive loss it

appears to be necessary to fashion almost all the probe out of a low conductivity material, e.g. ceramic.

To overcome these accumulated problems a third probe was constructed to measure the enthalpy flux. Simply stated, the new probe is a mass flux probe constructed primarily of ceramic material with a fine beaded thermocouple suspended within the probe directly behind the inlet pressure taps. In this fashion, the total temperature of the sample may be determined in the state of isokinetic sampling as well as the mass flux; from these quantities the total enthalpy flux may be deduced. As in all applications of the mass flux probe, the device is considered to operate as an integrating device and no detailed accounting of the fluctuations is obtained. However, experience with this probe, as will be evident from the results yet to be presented, indicates that the technique is basically sound and provides sufficient accuracy for most applications.

4. THE ISOTHERMAL HOMOGENEOUS JET

(A) *Experimental facility and exit conditions*

The constant density, or "cold jet", investigation was performed using a vertically oriented jet chamber. This facility was also used for the heated jet study and will be described in more detail in a subsequent section. The exit velocity was nominally 63 m/s and the exit profiles of mass and momentum flux were deduced from measurements using total and static pressure probes 0.45 mm in diameter. The mass flux probe previously was used for all other measurements.

(B) *Integral properties*

For a free jet the total momentum flux is conserved and thus the integral of the momentum flux data at any downstream station should be a constant. Figure 4 shows normalized results of direct numerical integration of the momentum flux data. Note that the total momentum flux is conserved within deviations of less than 9% of the initial value.

The mass flux measurements were performed simultaneously with the total head measurements to avoid errors due to incorrect probe positioning, etc. Direct numerical integration of the mass flux data yields the total mass flux of air at that location which, when compared to the initial mass flux of the jet, is a measure of the entrainment. The results for the integrated mass flux profiles are also shown in Fig. 4; the entrainment is found to assume a linear growth in the far field.

(C) *Centerline behavior of flux variables*

The centerline values of momentum flux, nondimensionalized with respect to the exit value, is shown in Fig. 5, for both experiment and the present theory. The data is seen to decay asymptotically as $\bar{x}^{-2}$ as expected. Note that the theoretical curve is plotted as a function of the transformed variable $\bar{\chi}$; of course, the initial profile used for the theoretical curve is that actually measured at the jet exit. By matching the centerline values of momentum flux a relation between $\bar{x}$ and $\bar{\chi}$ can be obtained. Such a relation may be found

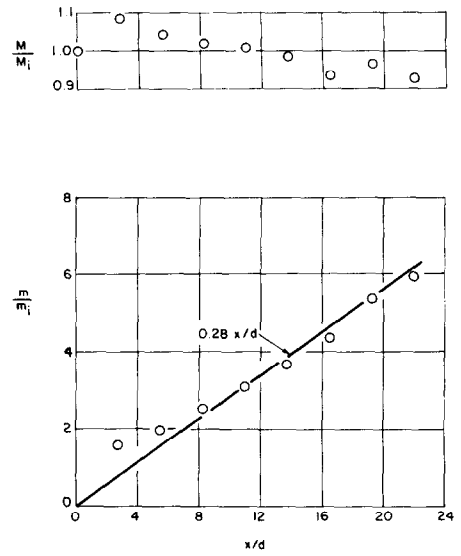

FIG. 4. Integral characteristics for cold jet. Upper graph shows variation of normalized integral of momentum flux with streamwise distance. Lower graph shows normalized mass entrainment variation with streamwise distance.

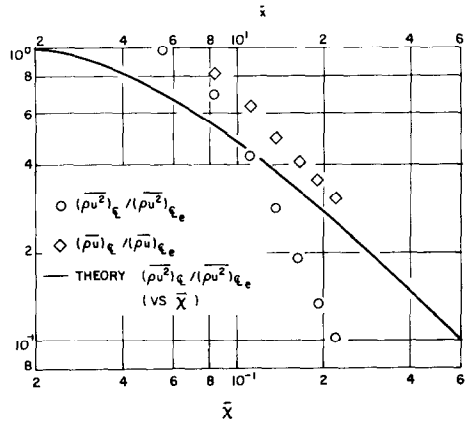

FIG. 5. Centerline characteristics for cold jet. Symbols are experimental data and are referred to $\bar{x}$ while the solid line is the theoretical result for centerline momentum flux and is referred to $\bar{\chi}$.

in other ways, e.g. by matching halfwidths, but the present method has proven to be both accurate and convenient.

Centerline values of mass flux of air are also shown in Fig. 5 and are seen to decay inversely with x/d in the far field; this is expected since the mass flux for this homogeneous case is proportional to the mean streamwise velocity. The mass flux is not a conserved quantity, and since a generation term for it in the describing equations has not been formulated, no theoretical results are given.

(D) *Halfwidths*

The halfwidths for all the flux variables are presented in Fig. 6 as a function of x/d. All the halfwidths are found to assume a linear growth with the constant of proportionality for the mass flux case equal to about 0.08; this value is consistent with typical mean velocity halfwidth results.

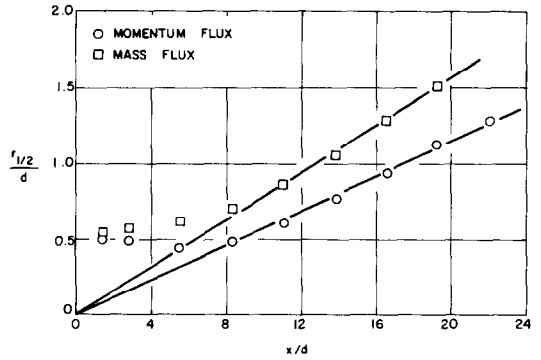

FIG. 6. Streamwise growth of the cold jet half-widths. Solid lines are added to illustrate linearity of data.

(E) *Theory compared to experiment*

The full solution for the momentum flux field of the isothermal homogeneous jet is compared to the experimental data in Fig. 7. The relation between $\bar{x}$ and $\bar{\chi}$ was obtained as explained previously. Note that the theory predicts the developing region accurately as well as giving a very good description of the far field region wherein similarity is achieved.

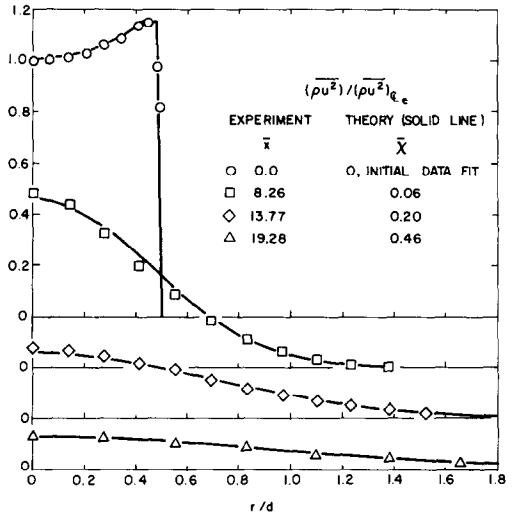

FIG. 7. Comparison of experiment and theory for momentum flux field of cold jet.

5. THE ISOTHERMAL, NONHOMOGENEOUS JET

(A) *Experimental facility and exit conditions*

The nonhomogeneous jet investigated consisted of carbon dioxide premixed with air to a molar concentration of 20% within the settling chamber. The mass flux probe described previously was used to measure the momentum flux, $\overline{\rho u^2}$, and the mass flux of carbon dioxide and of air, $\overline{\rho_C u}$ and $\overline{\rho_A u}$, respectively. A schematic diagram of the facility used is shown in Fig. 8. The exit velocity was about 63 m/s.

The exit profile of momentum flux was obtained by using 0.45 mm diameter pitot and static pressure tubes and a water manometer. The relatively large diameter of the mass flux probe did not permit accurate measurement of the exit profile of the species fluxes in the high shear region near the edge of the orifice. However, measurements over the central region of the jet in the plane of the orifice indicated that the CO_2 mass flux was constant. Since the gases were premixed and the flow at the exit plane is laminar, the density is fixed and the mass flux profiles at the exit is characterized by the profile of velocity. The total mass flux of CO_2 leaving the orifice calculated in this way was found to agree with that entering the settling chamber through the calibrated sonic orifice.

(B) *Integral properties*

For the nonhomogeneous jet, two integral quantities are conserved, namely the total momentum flux and the total mass flux of carbon dioxide. The results of a direct numerical integration of the raw data for these two quantities is shown in Fig. 9. The measurements indicate reasonably good conservation of these integral quantities, with deviations within 10% of the initial value.

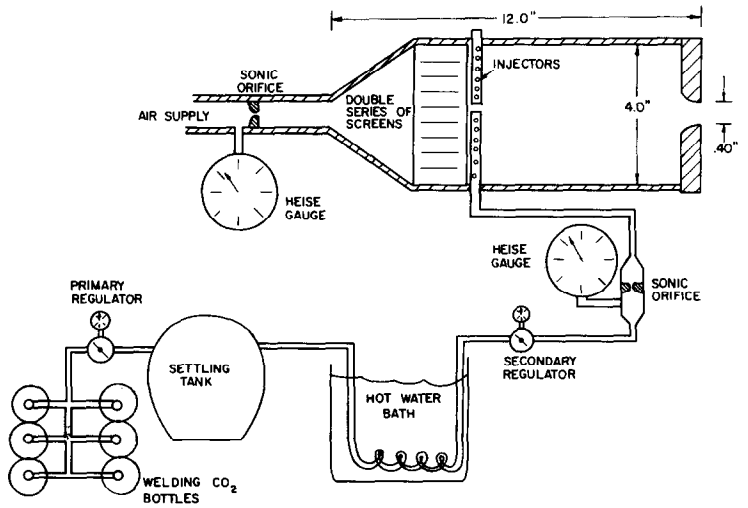

FIG. 8. Schematic diagram of the binary jet experimental facility.

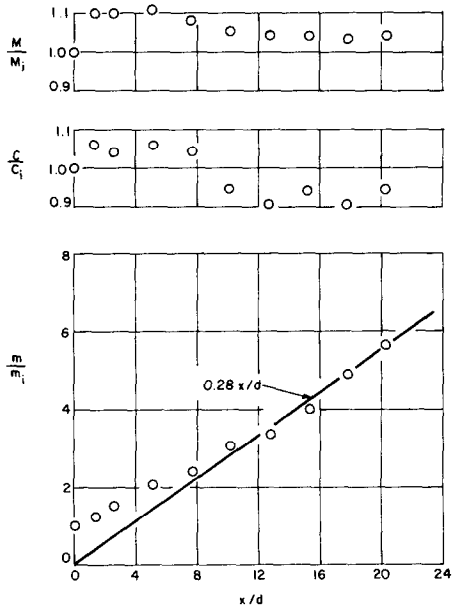

FIG. 9. Integral characteristics of the binary jet. The graphs show streamwise variation of total momentum flux, total carbon dioxide mass flux, and mass entrainment.

The remaining integral quantity of interest is the ratio of the total mass flux of air in the profile at any x station to the total mass flux of mixture at the jet exit. The result of numerical integration of the raw air flux data is presented in Fig. 9. The entrainment is found to asymptote to a linear growth, as expected.

(C) *Centerline behavior of flux variables*

The centerline value of momentum flux, mass flux of carbon dioxide, and mass flux of air, non-dimensionalized with respect to the centerline exit values, are plotted as a function of x/d in Fig. 10.

It is observed that the centerline values of momentum flux and of the mass flux of CO_2 decay as $x^{-2.00}$ far from the exit; however, the potential core length for the momentum flux is 6.7 diameters while that of the mass flux of CO_2 is 5.6 diameters. In this case, the initial profiles are nearly identical so that the more rapid decay of the CO_2 flux values is most likely not the result of initial conditions. By the conventional criteria for rates of mixing them, the mass flux of CO_2 would be said to mix faster than the momentum flux.

The theoretical behavior of the centerline values of momentum flux and mass flux of CO_2 are also presented in Fig. 10 plotted as functions of the transform variable $\bar{\chi}$. The difference in initial conditions for these two variables is so small that centerline behavior is almost indistinguishable in the transformed coordinate system.

As in the previous case, the $\bar{x}$ vs $\bar{\chi}$ transformations are obtained by matching centerline values of the dependent variables. The detailed results of this process will be discussed subsequently. It is sufficient, at this point, to note that two distinct transformations are generated, one for the momentum flux and the other for the mass flux of CO_2. These results, for the reasons discussed in Section 2, indicate that mass flux does indeed "mix" faster than momentum flux.

The centerline values of mass flux of air are also shown in Fig. 10 and are seen to decay inversely with x/d in the asymptotic limit. Because the total mass flux of air is not a conserved quantity, the theoretical development would require a source term in the air flux species equation. The approach to formulating such a source term has not yet been developed and thus no theoretical description for the air flux was obtained.

Another important conclusion results from the observed centerline behavior of the momentum flux. The present facility has also been used for homogeneous mixing studies. The momentum decay in the present study is found to be absolutely identical to that of previous homogeneous cases; thus the change in exit concentration in no way affects the momentum flux field.

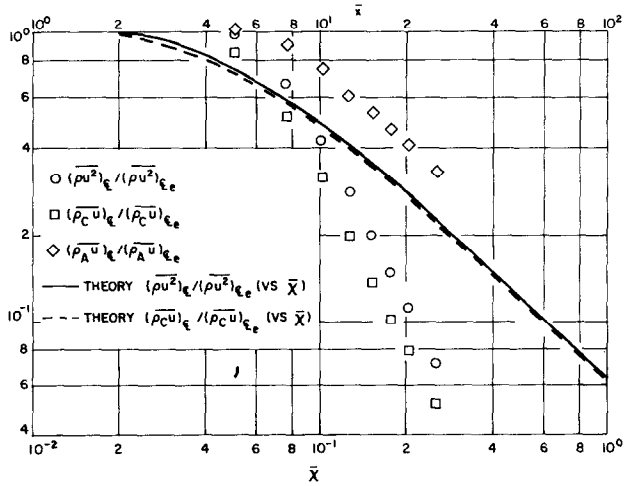

FIG. 10. Centerline characteristics for binary jet. Symbols denote experimental data and are referred to $\bar{x}$ while curves denote theoretical results and are referred to $\bar{\chi}$.

(D) *Halfwidths*

The halfwidths for all of the flux variables are presented in Fig. 11 as a function of x/d. All of the halfwidths are found to asymptote to a linear growth. Note that there is a small but distinct difference in the behavior of the halfwidths for the momentum flux and the mass flux of carbon dioxide. Following convention it can be said that the mass flux of CO_2 "mixes" faster than momentum flux in the sense that it has a larger halfwidth.

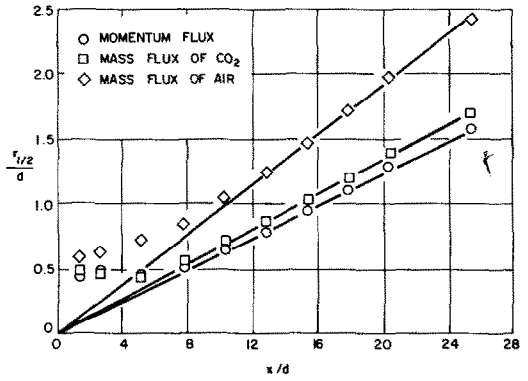

FIG. 11. Streamwise growth of binary jet halfwidths. Solid lines are added to illustrate linearity of data.

It is observed that the present experimental measurements indicate a preferential transport of mass flux over momentum flux in the sense that at a given x/d location, the centerline value of mass flux of CO_2 is lower than that of momentum flux and its halfwidth is larger. However, the measurements also indicate that the values of radial coordinate for which no sensible measurement of each variable is obtainable are identical for each flux variable. That is, the "edge" of the jet is the same for each quantity even though the mass flux of CO_2 has a larger value for its halfwidth and a lower centerline value than does the momentum flux. Previous experimental results, presented in terms of velocity and concentration, tended to indicate a different "boundary layer thickness" for each variable. The present results, however, show that all the flux variables are distributed differently in a mixing zone of apparently unique width.

The momentum halfwidths shown in Fig. 11 match exactly momentum halfwidths found in previous homogeneous cases; once again, it is found that for identical initial conditions, the momentum field is sensibly independent of the gas mixture.

(E) *Theory compared to experiment*

Using curve fits to the initial data and the $\bar{x}$ vs $\bar{\chi}$ transformation which shall be discussed subsequently, the complete analytic description of the momentum flux distribution and carbon dioxide mass flux distribution was generated. Figures 12 and 13 compare the theoretical and experimental results for the entire momentum flux and carbon dioxide mass flux field respectively. Note that the results are presented in terms of the physical coordinates, not similarity variables; also note that the theory reasonably predicts the developing region of the jet in addition to the fully developed region.

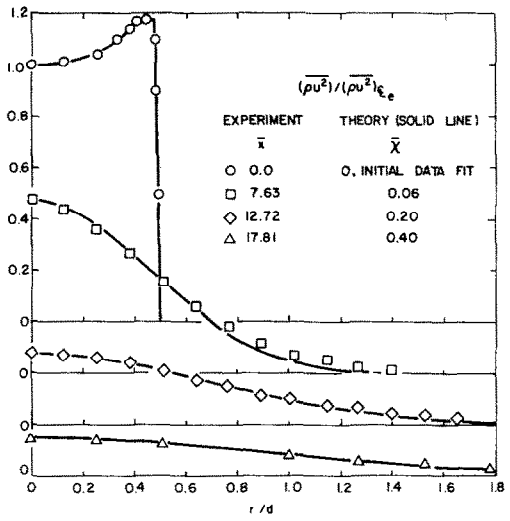

FIG. 12. Comparison of experiment and theory for momentum flux field of binary jet.

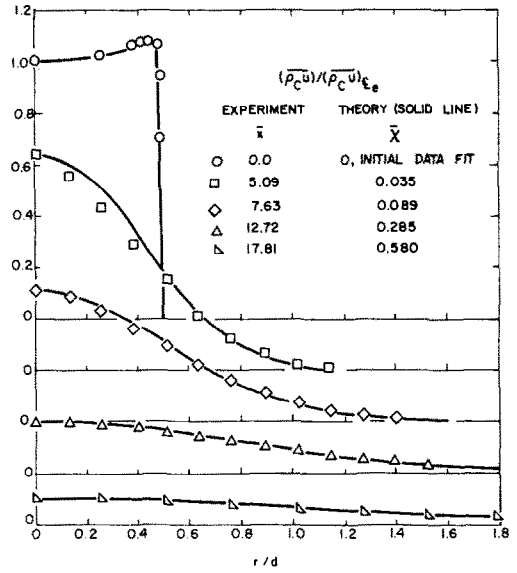

FIG. 13. Comparison of experiment and theory for carbon dioxide mass flux field of binary jet.

6. THE NON-ISOTHERMAL, HOMOGENEOUS JET

(A) *Experimental facility and exit conditions*

The non-isothermal jet facility exits vertically to avoid the asymmetries reported in [12] for horizontally flowing initially axisymmetric jets with densities different from the ambient density. The air supply is regulated and then passed through an electrical heater made from 4.7 mm dia nichrome wire; the temperature is regulated by a Capacitrol unit. The temperature of the air supply can be varied from room temperature to about 300°C. A schematic diagram of the homogeneous jet facility is shown in Fig. 14.

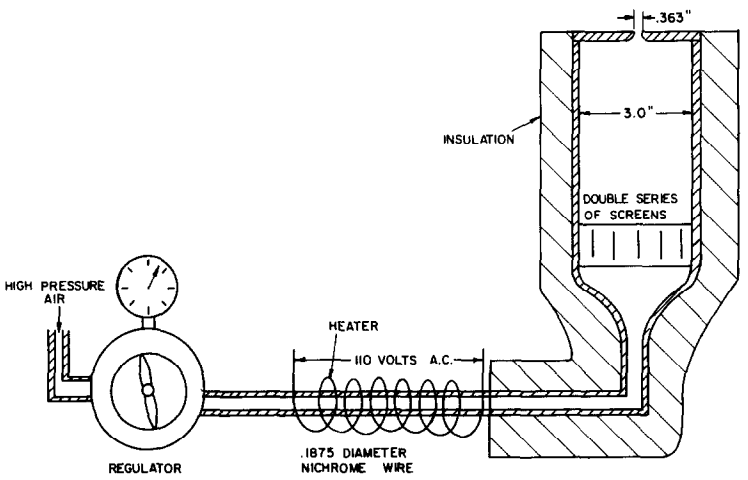

FIG. 14. Schematic diagram of experimental facility used for cold jet and hot jet investigations.

The nominal initial conditions for this investigation were a temperature of 150°C and an exit velocity of about 75 m/s. The exit profile of momentum flux was measured with 0.45 mm dia pitot and static tubes and water manometer. The exit profile of total enthalpy flux was computed from measurements of the pitot and static pressure and temperature measurements using a thermocouple.

(B) *Integral properties*

For the non-isothermal jet, two integral quantities are conserved; namely, the total momentum flux $\overline{\rho u^2}$ and the flux of the stagnation enthalpy less ambient enthalpy $\overline{\rho u(h_T - h_\infty)}$ which shall be referred to as enthalpy flux. The result of a direct numerical integration of the raw data for these two quantities is presented in Fig. 15. The measurements again indicate good conservation of total momentum flux and total enthalpy flux, within 10% at all locations.

The remaining integral quantity is the ratio of the total mass flux in the profile at any x station to the total exit mass flux. The results of numerical integration of the raw mass flux data are shown in Fig. 15. The entrainment is found again to asymptote to a linear growth. A comparison of the mass entrainment properties of all the jets examined will be presented subsequently.

(C) *Centerline behavior of flux variables*

The centerline values of momentum flux, enthalpy flux, and mass flux, nondimensionalized with respect to the exit values are plotted as a function of x/d in Fig. 16. It is observed that the centerline values of the momentum flux and the enthalpy flux decay as $\bar{x}^{-2}$ far from the exit; however, the potential core for the momentum flux is 6.9 diameters while that of the enthalpy flux is 5.5 diameters. In this case, the initial profile of the enthalpy flux is considerably less "full" than that of momentum flux so that it is expected that the enthalpy flux should decay faster, and it would, therefore, be difficult to unambiguously compare the rates of mixing between the two.

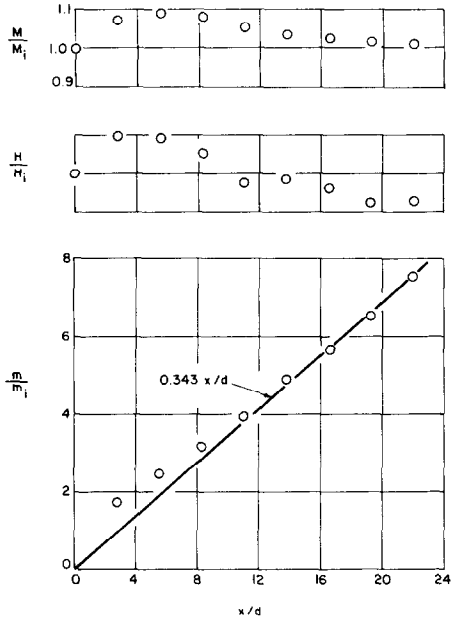

FIG. 15. Integral characteristics of the hot jet. The graphs show streamwise variation of total momentum flux, total enthalpy flux, and mass entrainment.

The theoretical behavior of the centerline values of momentum flux and enthalpy flux, plotted as a function of the transform variable $\bar{\chi}$, are shown in the same figure. The difference in initial conditions for these two variables is seen to manifest itself as a shift between the two curves.

As was done previously, the $\bar{x}$ vs $\bar{\chi}$ transformations are obtained by matching centerline values of the dependent variables. The results of this technique are discussed in detail subsequently. Similar to the non-homogeneous jet, two distinct transformations are generated for momentum flux and enthalpy flux. The results indicate that enthalpy flux "mixes" faster than momentum flux. Note that this comparison can be made despite the difference in initial conditions.

The centerline values of mass flux are also presented in Fig. 16 and they are seen to decay linearly with x/d in

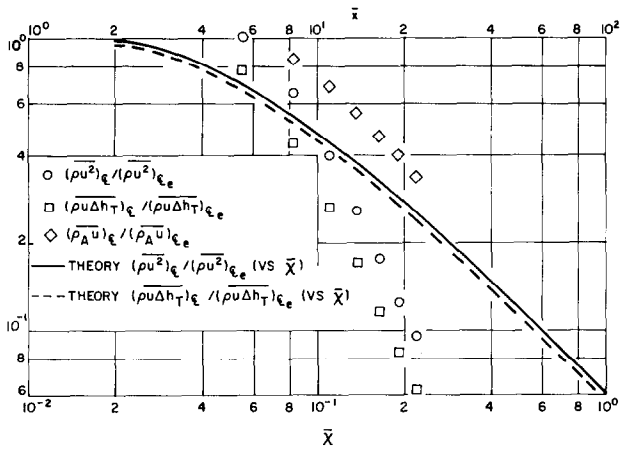

FIG. 16. Centerline characteristics for hot jet. Symbols denote experimental data and are referred to $\bar{x}$ while curves denote theoretical results and are referred to $\bar{y}$.

the asymptotic limit of large $\bar{x}$. Since the total mass flux is not conserved, no theoretical solution was developed.

An important conclusion obtained from the centerline behavior of momentum flux is that it is not affected by heating so long as the initial conditions on momentum flux remain the same. Note that there is no appreciable difference in momentum flux behavior between the isothermal nonhomogeneous jet (refer to Fig. 10) or the non-isothermal homogeneous jet (refer to Fig. 16).

(D) *Halfwidths*

The halfwidths for all the flux variables are presented in Fig. 17 as a function of x/d. All of the halfwidths are found to asymptote to a linear growth. Note that the enthalpy flux halfwidths are distinctly larger than the corresponding momentum flux halfwidths so that in this sense, it can be said that enthalpy flux "mixes" faster than momentum flux.

It is observed that the present experimental measurements indicate a preferential transport of energy over momentum in the sense that at a given value of x/d, the centerline value of enthalpy flux is lower than that of momentum flux and its halfwidth is larger. However, the measurements again indicate that the values of radial coordinate for which no sensible measurement of each variable is obtainable is identical for each flux variable. That is, the "edge" of the jet is the same for each quantity even though the enthalpy flux has a larger halfwidth and a lower centerline value than does the momentum flux. Previous experimental results presented in terms of velocity and temperature, tended to indicate a different "boundary-layer thickness" for each variable. The present results, however, show that the flux variables are distributed differently in a mixing zone of apparently unique width.

(E) *Theory compared to experiment*

Using the $\bar{x}$ vs $\bar{y}$ transformations, the complete analytic description of momentum flux and enthalpy flux was generated. Figure 18 compares the theoretical and experimental results for the entire momentum flux field of the non-isothermal jet. Figure 19 compares the theoretical and experimental results for the entire enthalpy flux field. Note that the results are presented in terms of physical coordinates, not similarly variables, and that the theory adequately predicts the developing region of the jet in addition to the fully developed region.

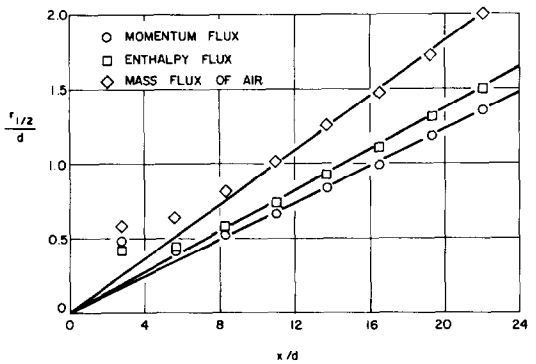

FIG. 17. Streamwise growth of hot jet halfwidths. Solid lines are added to illustrate linearity of data.

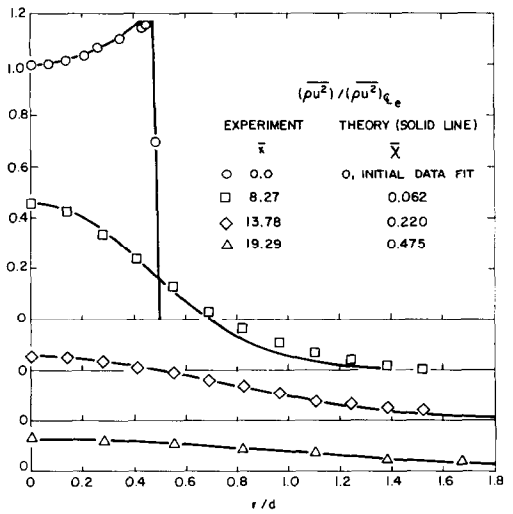

FIG. 18. Comparison of experiment and theory for momentum flux field of hot jet.

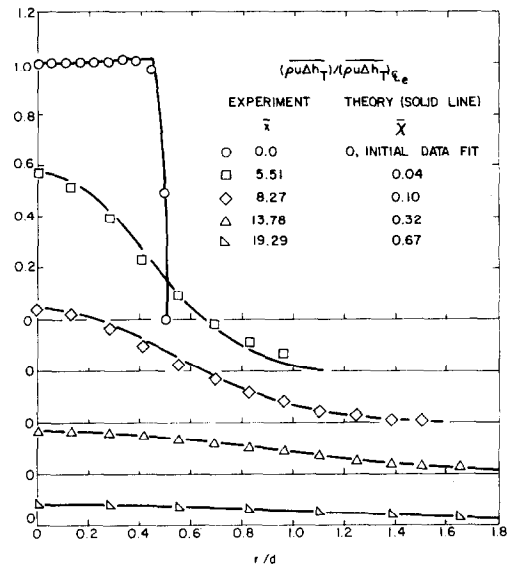

FIG. 19. Comparison of experiment and theory for enthalpy flux field of hot jet.

7. FURTHER RESULTS

(A) *The coordinate transformation*

In all the cases presented here the centerline properties of the conserved flux variables have been matched to those obtained analytically in order to effect a relationship between the physical coordinate $\bar{x}$ and the transformed coordinate $\bar{\chi}$. The hypothesis of this extended Reichardt free-mixing theory is that a unique relationship exists between the two, i.e. there is a unique $\Lambda(x)$ for identical mixing processes. The data to support this hypothesis is shown in Fig. 20 where it is clear that all the data for momentum flux matching fall essentially upon one curve while all the data for mass flux and enthalpy flux matching fall together upon a second curve.

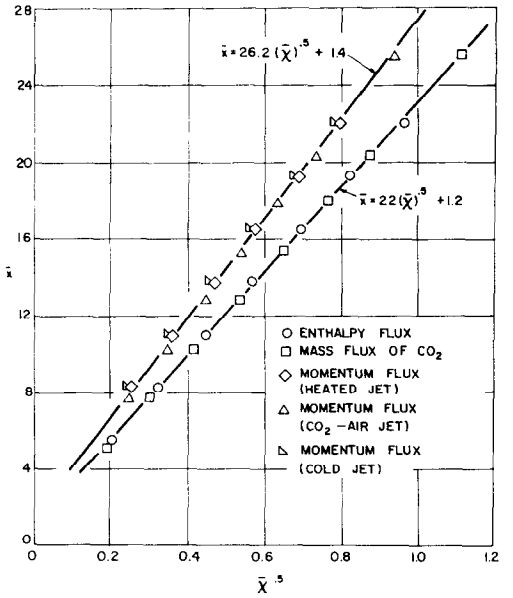

FIG. 20. Correlation of physical and transformed coordinates for all cases tested. Upper curve is for momentum flux and lower curve for enthalpy flux and carbon dioxide mass flux.

It is suggested then that mass and enthalpy mixing are identical processes distinct from the process of momentum mixing. In addition, the coordinate relations shown (or the use of $\Lambda = d\bar{\chi}/d\bar{x}$ obtained from the data) should be useful for determining the mass, momentum, and enthalpy flux fields for axisymmetric free jet mixing flows when the initial conditions are known.

(B) *Mass entrainment correlation*

All the data for mass entrainment (normalized with respect to the total exit mass flux) is quite well correlated by the reduced coordinate $(\rho_x/\rho_e)^{1/2}x/d$ as shown in Fig. 21. This correlation may be approximated as

$$m/m_i = 0.28(\rho_x/\rho_e)^{1/2}x/d$$

for

$$(\rho_x/\rho_e)^{1/2}x/d > 10$$

for the nonuniform as well as the uniform jets tested.

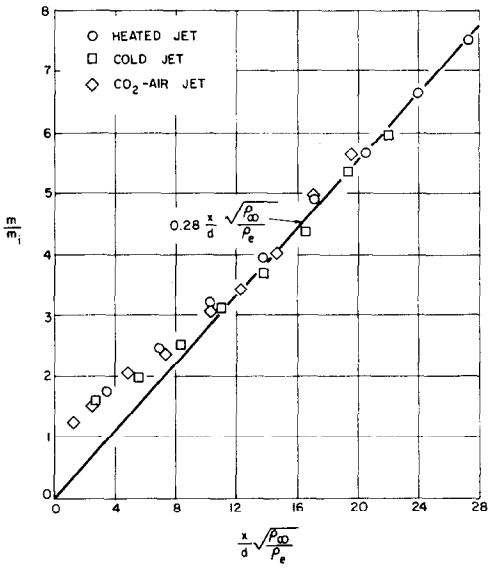

FIG. 21. Correlation of mass entrainment data for all jets investigated.

The commonly accepted coefficient for the correlation equation is 0.32 obtained by Ricou and Spalding [13] as a result of an ingenious experiment which obviated the need for profile integration. However, their data is for the far field of axisymmetric jets, $x/d > 25$ and in the near field as studied here more diversity in the magnitude of this coefficient is observed among various researchers.

(C) *Behavior of the conventional flow variables*

The centerline behavior of the velocity, total temperature, and concentration deduced from the raw data for all cases tested is shown in Fig. 22. It should be noted that the so-called momentum diameter $\theta =$

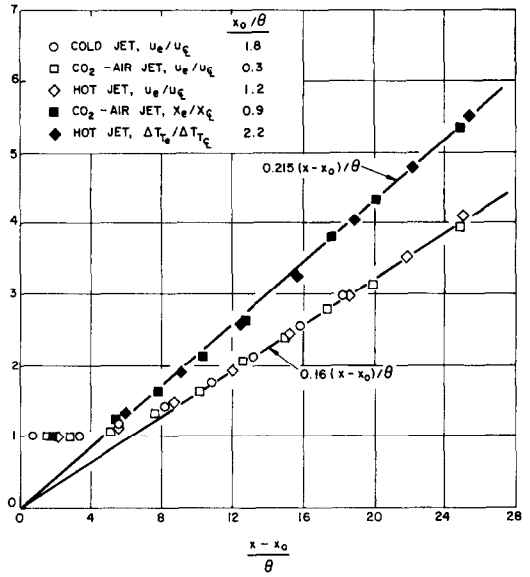

FIG. 22. Correlation of centerline properties of conventional variables for all jets investigated. Straight lines added to illustrate data trend.

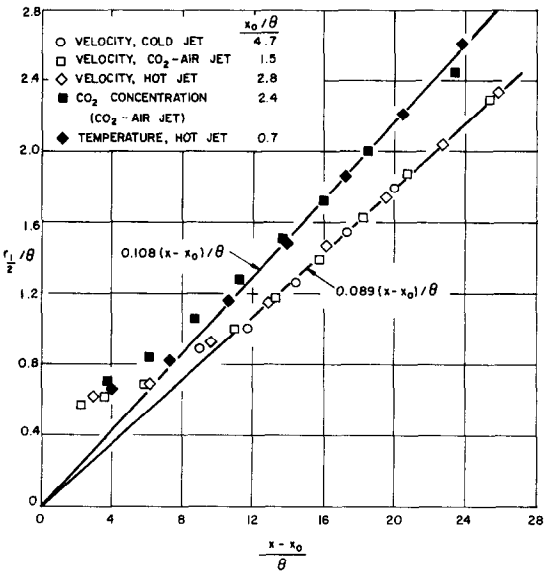

FIG. 23. Correlation of halfwidths of profiles of conventional variables for all jets investigated. Straight lines added to illustrate data trend.

$(\rho_\infty/\rho_e)^{-1/2}d$ properly scales the axial coordinate and that the normalized temperatures and concentrations follow one curve while the normalized velocities follow another. The data are seen to assume linear behavior in the far field, as expected. The straight lines faired through the data are characterized by slopes which are in good agreement with previous investigations. For example, Becker *et al.* [14], in their study of the concentration field of a round jet, reviewed the results of eleven other reports on the concentration and/or temperature fields of round jets. The average value of the reported slopes of the temperature or concentration curves is 0.204 while for the present study it is 0.215. Six of the eleven studies cited gave velocity results with an average slope of 0.158 compared to the present value of 0.160.

In the same fashion the halfwidths for velocity, temperature, and concentration are scaled by the momentum diameter. Here again, the temperature and concentration fields spread identically and at a faster rate than the velocity field, as shown in Fig. 23. The average value of the temperature or concentration half-width slope, as reported by [14], is 0.102 and in the present study it is 0.108. The velocity half-width slope has an average value of 0.087 while here it is 0.089. Again it is seen that the results of the present work, in terms of conventional variables, is in good agreement with previous investigations.

Acknowledgements—This research was supported in part under Contract No. Nonr 839(38) for Project Strategic Technology, by the Advanced Research Projects Agency under Order No. 529 through the Office of Naval Research; in part under Contract No. DAHCO4-69-C-0077, monitored by the U.S. Army Research Office under ARPA Order No. 1442; and partly by the Advanced Research Projects Agency of the Department of Defense, monitored by ONR under Contract No. N00014-67-A-0438-0017. Portions of this report were based on the dissertation of the second author, presented to the Polytechnic Institute of Brooklyn in partial fulfillment of the requirements for the degree of Ph.D. (Aeronautics and Astronautics), 1971.

The authors gratefully acknowledge the encouragement and helpful comments of Professor Martin H. Bloom.

REFERENCES

1. S. N. B. Murthy (editor), *Proceedings of SQUID Workshop on Reacting and Nonreactioning Turbulent Flows.* Project SQUID Report, Purdue University (1974).
2. *Free Turbulent Shear Flows*, Proceeding of a conference held at NASA-Langley, 20–21 July 1972, NASA SP-321 (1972).
3. *Turbulent Shear Flows*, Proceedings of an AGARD Conference, London, 13–15 September 1971. AGARD CP-93 (1971).
4. G. L. Brown and A. Roshko, On density effects and large structure in turbulent mixing layers, *J. Fluid Mech.* **64**(4), 775–816 (1974).
5. D. B. Spalding, Concentration fluctuations in a round turbulent free jet, *Chem. Engng Sci.* **26**, 95–107 (1971).
6. J. Laufer, On turbulent shear flows of variable density, AIAA paper No. 68-41, AIAA 6th Aerospace Sciences Meeting, New York (January 1968).
7. J. Way and P. A. Libby, Application of hot-wire anemometry and digital techniques to measurements in a turbulent helium jet, *AIAA Jl* **9**(8), 1567–1573 (1971).
8. A. E. Davis, Spread of a heated plane turbulent jet, *Physics Fluids* **18**(7), 770–775 (1975).
9. H. Reichardt, On a new theory of free turbulence, *Z. Angew. Math. Mech.* **21**(5), 257–264 (1941).
10. T. Baron and L. G. Alexander, Momentum, mass and heat transfer in jets, *Chem. Engng Prog.* **47**(4), 181–185 (1951).
11. I. Wygnanski and H. E. Fiedler, Some measurements in the self-preserving jet, Boeing Scientific Research Laboratories Document D1-82-0712 (April 1968).
12. N. Trentacoste and P. M. Sforza, Studies in homogeneous and nonhomogeneous free turbulent shear flows, PIBAL Rept. 69-36 (1969).
13. F. P. Ricou and D. B. Spalding, Measurements of Entrainment by axisymmetric turbulent jets, *J. Fluid Mech.* **11**(1), 21–32 (1961).
14. H. A. Becker, H. C. Hottel and G. C. Williams, The nozzle-fluid concentration field of the round, turbulent, free jet, *J. Fluid Mech.* **30**(2), 285–304 (1967).

TRANSPORT DE MASSE, DE QUANTITE DE MOUVEMENT, D'ENERGIE DANS LES JETS LIBRES TURBULENTS

Résumé—On présente une étude expérimentale et analytique du transfert de masse, de quantité de mouvement et de chaleur dans un écoulement turbulent et libre. On étudie en particulier le cas d'un jet issu d'un orifice circulaire et entrant dans l'atmosphère d'une salle de laboratoire. On considère trois conditions d'écoulement: (1) mélange isotherme d'un jet d'air avec l'environnement, (2) mélange isotherme d'un jet de mélange binaire (air/CO_2) avec l'environnement, (3) mélange non isotherme d'un jet d'air chaud avec l'environnement. Des sondes à aspiration spécialement conçues sont utilisées pour mesurer les flux moyens de masse, de quantité de mouvement et d'enthalpie. Ces propriétés sont considérées comme les variables dépendantes définissant le champ d'écoulement. Des estimations précises des variables plus usuelles telles que fraction molaire moyenne d'espèces, vitesse massique moyenne et température moyenne sont déduites des résultats bruts des échantillons aspirés. Les résultats normalisés indiquent que, pour des conditions initiales identiques les flux de masse et d'enthalpie totale sont identiques et que ces deux variables décroissent plus vite et ont des demi-largeurs plus épaisses que le flux de quantité de mouvement. Néanmoins la coordonnée radiale à laquelle la valeur de la variable flux est sensiblement égale à zéro, c'est à dire le "bord" moyen du jet, est trouvée être la même pour tous les flux.

On propose une version élargie de la théorie inductive de Reichardt pour la turbulence libre afin de prédire correctement le champ complet dans l'écoulement des variables de flux.

STOFF-, IMPULS- UND ENERGIETRANSPORT IN TURBULENTEN FREISTRAHLEN

Zusammenfassung—Es wird eine experimentelle und analytische Studie über den Stoff-, Impuls- und Wärmeübergang in einem Feld freier turbulenter Strömung vorgelegt. Insbesondere wird der Fall des aus einer Düse mit kreisförmigem Querschnitt in die freie Umgebungsatmosphäre eines Laborraumes austretenden Strahles untersucht. Die grundlegenden Strömungsbedingungen werden betrachtet: (1) isotherme Mischung des Strahles mit der Umgebung; (2) isotherme Mischung eines Strahles aus einem binären Gemisch (Luft/Co_2) mit der Umgebung; (3) nichtisotherme Mischung eines geheizten Luftstrahles mit der Umgebung. Speziell konstruierte Aspirationssonden werden zur Messung der mittleren Ströme von Masse, Impuls und totaler Enthalpie verwendet. Diese Größen werden als die das Strömungsfeld definierenden abhängigen Variablen betrachtet. Genaue Werte der gebräuchlichen Größen, wie des mittleren Molanteils, der mit den Massenanteilen gemittelten Geschwindigkeit und der mittleren Temperatur fallen als Nebenprodukte der mit den Aspirationssonden gewonnenen Meßdaten an. Die dimensionslos gemachten Ergebnisse zeigen, daß sich bei identischen Anfangsbedingungen die Ströme von Masse und totaler Enthalpie identisch verhalten und daß diese beiden Größen schneller abnehmen und größere Halbwertbreiten haben als der Impulsstrom. Die radiale Koordinate jedoch, bei welcher die Stromvariable praktisch gleich null ist, d.h. die mittlere Strahlgrenze, ist für alle Stromvariablen identisch. Es erweist sich, daß eine erweiterte Version der Theorie der freien Turbulenz von Reichardt das gesamte Strömungsfeld bezüglich aller konservativen Stromvariablen angemessen beschreibt.

ПЕРЕНОС МАССЫ, КОЛИЧЕСТВА ДВИЖЕНИЯ И ЭНЕРГИИ В ТУРБУЛЕНТНЫХ СВОБОДНЫХ СТРУЯХ

Аннотация — Проведено экспериментальное и аналитическое исследование переноса массы, количества движения и тепла в свободном турбулентном потоке. В частности, изучается случай струи, истекающей из круглого отверстия в окружающую атмосферу лабораторного помещения. Рассматриваются три основных режима течения: (1) изотермическое смешение воздушной струи и окружающей среды; (2) изотермическое смешение струи бинарной смеси (воздух—CO_2) с окружающей средой; (3) неизотермическое смешение струи нагретого воздуха с окружающей средой. Для измерения средних потоков массы, количества движения и общей энтальпии используются специально созданные аспираторные датчики. Считают, что эти характеристики являются зависимыми переменными, определяющими поле течения. По необработанным данным для аспираторных датчиков определяют также точные значения таких обычно используемых параметров, как средне-объемная мольная концентрация, средне-массовая средняя скорость и средняя температура.

Полученные результаты показывают, что при идентичных начальных условиях поведение потока массы и потока общей энтальпии одинаково и что обе эти переменные стремятся к нулю быстрее и имеют большую полуширину, чем поток количества движения. Найдено, однако, что радиальная координата, при которой величина переменной потока практически равна нулю (т. е. средний «край» струи) одинакова для всех переменных потока.

Найдено, что обобщенный вариант индуктивной теории свободной турбулентности Райхардта удовлетворительно описывает поле течения для всех переменных установившегося потока.